VISUALIZATION OF JET FLOW IN A MIXING VESSEL WITH A NOZZLE ROTATING AROUND THE VESSEL AXIS

SEUNG TAE KOH, SETSURO HIRAOKA, YUTAKA TADA,
TSUTOMU ARAGAKI, TOSHIHARU HIJIKATA AND TAKAO YAMAGUCHI
Department of Applied Chemistry, Nagoya Institute of Technology, Nagoya 466

Key Words: Jet Mixing, Rotating Nozzle, Flow Visualization, Streak Line, Flow Pattern

Jet flow in a mixing vessel equipped with a nozzle rotating around an inner shaft which has the same axis as the vessel was visualized with a tracer technique. The expanding jet angle was measured to be 21°–24° regardless of the jet flow rate. The effects of the angle, rotating speed and direction of rotation of the nozzle on the flow pattern was observed, and the relation of flow pattern to mixing time was evaluated in reference to the measured mixing time reported in our previous paper. The minimum dimensionless mixing time occurred when the streak line of the jet turned smoothly from the radial direction to the tangential one by the rotation of the inner shaft, without impingement of the jet on the vessel wall.

To estimate the flow pattern under optional conditions, a correlation equation of the streak line of the jet was derived theoretically from the differential equations of the radial and tangential velocity components of the jet.

Introduction

Flow patterns in mixing vessels have a great effect on mixing time and heat transfer coefficient. In the previous papers[6,7] the mixing time and heat transfer coefficient in the cylindrical jet mixing vessel were reported under various conditions (nozzle angles, jet flow rates, nozzle rotation speeds and nozzle rotation directions) that affected the flow patterns. The precise flow patterns depend on the physical properties of the fluid, the mixing operation conditions and the overall vessel configuration.

There have been many investigations for visualization of the jet flow[8,10] and of the flow in the mixing vessel[9,11,15] using tracer techniques. However, the flow pattern in a jet mixing vessel with a nozzle rotating around the vessel axis is not clear.

The aim of this work is to make that flow pattern clear, along with the relation of the pattern to the mixing time, using flow visualization. Jetted liquid configurations, including a bounded jet and an angular radial jet, are visualized with a tracer. A correlation equation for a streak line of the jet flow is derived from differential equations of the radial and tangential

* Received April 10, 1991. Correspondence concerning this article should be addressed to S. Koh. T. Yamaguchi is now at Chubu University, Kasugai 487.

velocity components of the jet.

1. Experimental

Figure 1 shows a schematic diagram of the experimental apparatus. The vessel dimensions and the liquid circulation system are exactly the same as discribed in the previous paper[6]. Red ink was injected through a tracer filling line into the vessel with three-way valves in a very short impulse. From that monent the shutter of a camera was released to take photographs at intervals of 0.29 second. The camera used was a motor-driven Nikon FE with an exposure time of 1/250 second and a lens aperture of f5.6 under the lighting of two 500-watt bulbs.

2. Results and Discussion

2.1 Visualization of jet flow

Figure 2 shows side views of the jet formed by injecting red ink for a 0° nozzle angle without nozzle rotation. The injected ink expanded with an angle of 21°–24° regardless of the jet flow rate. This angle is close to the 26° of Pearce[12] and Ferguson[3], 22° of Lane and Rice[9] and 20° of Folson[4] and Sato[15].

The radial jet turned into a bounded jet on the vessel wall, consisting of bounded tangential and vertical jet components along the vessel wall. The bounded jet was symmetrical around the stagnation point of the jet on the wall and the magnitude of bounded jet flow was proportional to the jet flow rate.

Figure 3 shows top views of the jet flow for a 0° nozzle angle with nozzle rotation. The jet flow was angular and radial in nature by the combination of nozzle rotation speed and jet velocity. The jet flow at high jet velocity and low nozzle rotation speed, ②, took a radial flow pattern and then became a bounded jet after impinging on the vessel wall. The jet flow at low jet velocity and high nozzle rotation speed, ④, took an angular flow and then became tangential flow without impingement.

Figure 4 shows top views of the jet flow for a nozzle angle of 30° with nozzle rotation. The nozzle angle at

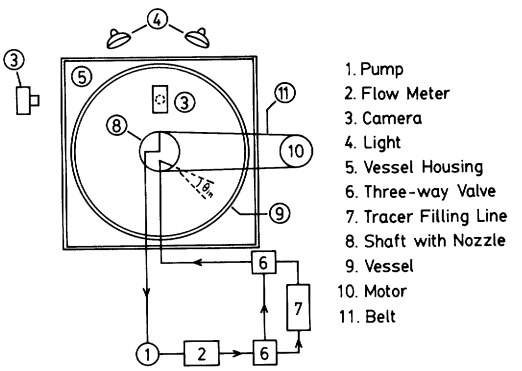

Fig. 1. Schematic diagram of experimental apparatus

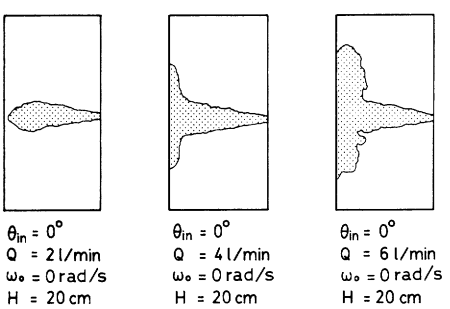

Fig. 2. Side view of jet flows for 0° nozzle angle

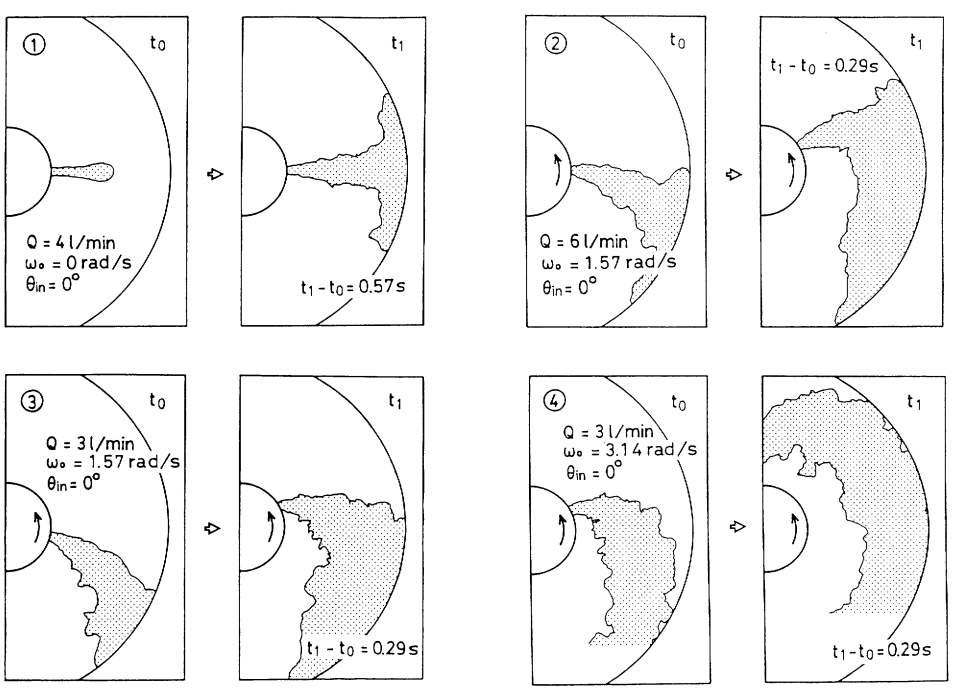

Fig. 3. Top view of jet flows for 0° nozzle angle

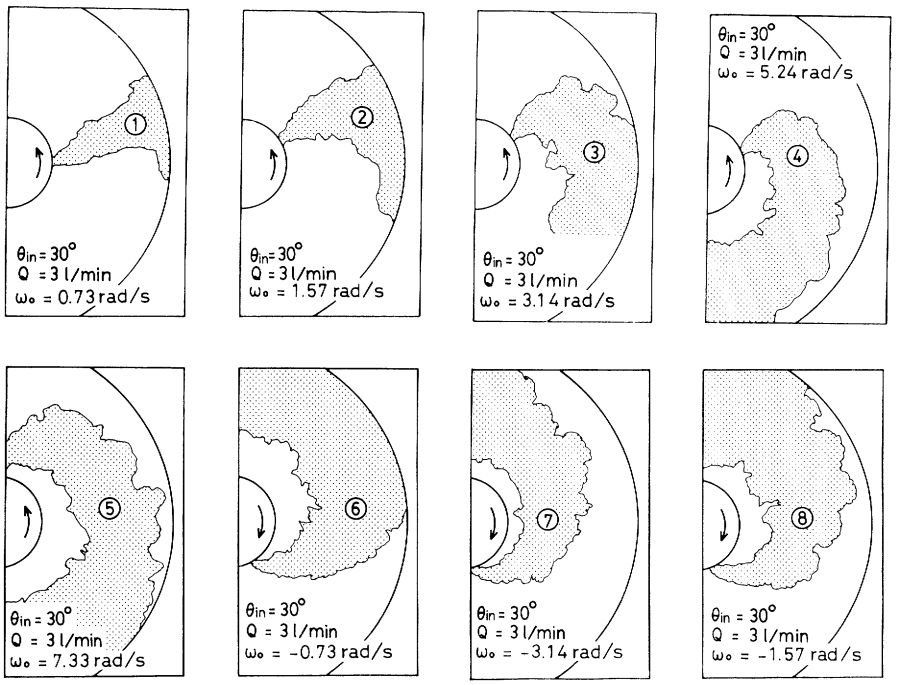

Fig. 4. Top view of jet flows for 30° of nozzle angle

30° produced more tangential flow in negative nozzle rotation (reverse rotation against the nozzle direction) than that at 0° due to its angle. Therefore, for correlation between the dimensionless mixing time t_M/t_R and the dimensionless nozzle rotation speed Ω^*, the axis of Ω^* for the symmetry of the correlation line shifted to the positive side with a value of 0.055, as described in the previous paper[6] (see also **Fig. 5**).

The numbers on the correlation line between t_M/t_R and Ω^* in Fig. 5, which represents the relation of the flow pattern to the mixing time, are the numbers of the visualized flow patterns indicated in Figs. 3 and 4. The dimensionless mixing time for the 0° nozzle angle reached its largest value at 6 *l*/min and 1.57 rad/s, ②, and decreased with increasing or decreasing Ω^*.

This fact can be explained by the effect of the bounded jet. At 0 rad/s the bounded jet is divided into bounded vertical and tangential jets of almost equal magnitudes. With nozzle rotation, however, the bounded vertical jet weakens and the front part of the bounded tangential jet in the direction of nozzle rotation interferes with the successive radial jet's impingement on the vessel wall. Consequently, the mixing efficiency is lowered and the dimensionless mixing time increases. The contrary effect of nozzle rotation on mixing time becomes maximum at $\Omega^* = 0.02$, and beyond this value of Ω^* the contrary effect begins to vanish and the tangential free jet grows to become the dominant flow in the mixing vessel. The same results are observed in the case of the 30° nozzle angle.

Reverse rotation against the nozzle direction gives

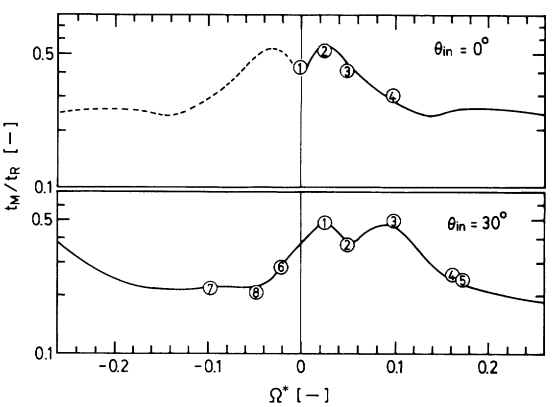

Fig. 5. Flow visualization points on correlation line of dimensionless mixing time t_M/t_R with respect to Ω^*

the minimum dimensionless mixing time at smaller $|\Omega^*|$ than does the positive rotation, as shown in ⑦ and ⑧ in Fig. 5. This fact can be considered to occur because the jet flow injected in the reverse direction of nozzle rotation is assisted by a relative tangential flow to inner shaft rotation, and then becomes an angular tangential jet without the appearance of the bounded jet.

2.2 Streak line of jet in a vessel with a rotating nozzle

In this section we predict quantitatively how to bend the radial jet in a tangential direction. To deal mathematically with such a problem, the bent flow pattern of the jet must be replaced by a representative line (a center line of the jet—a streak line of the jet). As shown in **Fig. 6**, suppose that the inner shaft is rotating at an angular velocity ω_0 and the nozzle is

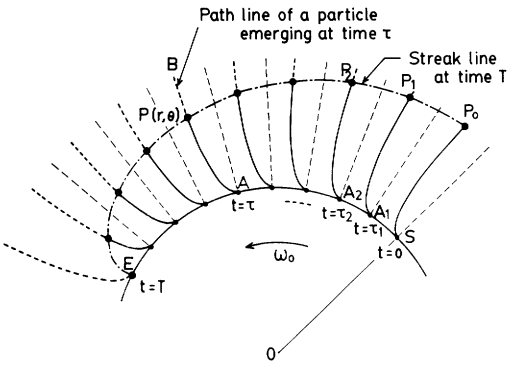

Fig. 6. Relation between streak line and path line

continuously ejecting non-colored water into the vessel, and that just at the moment ($t=0$) when the nozzle exit reaches point S, colored water begins coming out of the nozzle exit.

Let points $S, A_1, A_2, \cdots, A, \cdots, E$ be the positions of the moving nozzle at the times $t=0, \tau_1, \tau_2, \cdots, \tau, \cdots, T$, respectively. At each of these positions, a small amount of colored water, i.e., a fluid particle, is ejected, and each of these particles travels along a particular trajectory as shown in Fig. 6. To avoid ambiguity we distinguish each of these fluid particles by specifying the time τ, and use the notation "the particle (τ)". Particle (τ_i) leaves point A_i at time $t=\tau_i$ and travels along the curved line A_iP_i. To formulate the equation of the trajectory curve APB (i.e., path line) for particle (τ), we use the polar coordinate system with base line OS and with point O as the pole. To determine path line APB, a fundamental assumption is made about the velocity vector of the particle (τ) as

$$\boldsymbol{v}=f(r)\boldsymbol{e}_r+g(r)\boldsymbol{e}_\theta \tag{1}$$

where $f(r)$ is the radial velocity component and $g(r)$ the tangential velocity component. This assumption implies that the momentum of particle (τ) depends only on the radial distance; and that the path lines for different τ's are closely similar in their shapes. The above equations is equivalent to the following equation set:

$$\frac{dr}{dt}=f(r) \tag{2}$$

$$\frac{rd\theta}{dt}=g(r) \tag{3}$$

Taking into account that particle (τ) leaves point A ($r_0, \omega_0\tau$) at time τ, the initial condition must be

$$r=r_0 \quad \text{and} \quad \theta=\omega_0\tau \quad \text{at} \quad t=\tau \tag{4}$$

The position $P(r, \theta)$ of particle (τ) at an arbitrary time $t=t$ can be determined by integrating Eqs. (2) and (3) over the time range $[\tau, t]$ under the condition of Eq. (4). Then the relations become as follows:
for the radial distance r,

$$\int_{r_0}^{r}\frac{dr}{f(r)}=t-\tau \tag{5}$$

and for the angle θ,

$$\theta-\omega_0\tau=\int_{r_0}^{r}\frac{g(r)dr}{rf(r)} \tag{6}$$

When τ is fixed so as to specify a fluid particle, the above equations give the position $P(r, \theta)$ of particle (τ) at any time t, i.e., the trajectory curve of the particle (τ). Trajectories corresponding to different particles are schematically shown by solid lines in Fig. 6. On the contrary, when the time t is fixed at $t=T$, the set of Eqs. (5) and (6) gives the positions $P_i(r, \theta)$'s corresponding to different τ_i's (i.e., different particles) at the fixed time T. Then, combining Eqs. (5) and (6), and eliminating τ, the relation of the streak line at time T becomes

$$\theta=\omega_0 T-\int_{r_0}^{r}\frac{1}{f(r)}\left[\omega_0-\frac{g(r)}{r}\right]dr \tag{7}$$

For the radial velocity component $f(r)$ of fluid particle (τ) on the corresponding path line, the following equation is used as a first approximation.

$$f(r)\equiv V_r\equiv\frac{dr}{dt}=K\cdot\frac{r_0}{r}V_j\cos\theta_{in} \tag{8}$$

where K is a correction factor, and V_j and θ_{in} denote the jet velocity at the nozzle exit and the jet angle, respectively.

Equation (8) is principally based on the fact that when the inner shaft is at rest and the jet direction is perpendicular to the surface of the inner shaft, the axial centerline velocity is similar to that of the normal jet flow[1,7,11], though Eq. (8) is corrected for the nozzle angle. Equation (8) needs more correction because the inner shaft is rotating and the jet direction is not perpendicular to the surface of the inner shaft, and because vertical and tangential diffusions which are mainly caused by jet entrainment must be taken into account. We simply assume that a correction factor K is given by

$$K=\exp\left[-K_0\left(\frac{r-r_0}{R_0-r_0}\right)\right] \tag{9}$$

where K_0 depends on nozzle angle and angular velocity and the value of K_0 is determined so as to fit the experimental results. Combining Eqs. (8) and (9), we get

$$f(r)\equiv V_r=\left[\exp\left\{-K_0\left(\frac{r-r_0}{R_0-r_0}\right)\right\}\right]\times\left(\frac{r_0}{r}\right)V_j\cos\theta_{in} \tag{10}$$

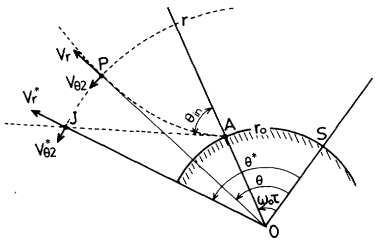

Fig. 7. Velocity components V_r, $V_{\theta 2}$ on path line and corresponding velocity components V_r^*, $V_{\theta 2}^*$ on straight jet line

For simplicity, the tangential velocity component $V_\theta \equiv g(r)$ is assumed to be decomposed into two parts $(V_{\theta 1}, V_{\theta 2})$; $V_{\theta 1}$ is the rotating flow induced by the rotation of the inner shaft; $V_{\theta 2}$ is the tangential flow induced by the jet flow.

$$V_\theta \equiv g(r) = V_{\theta 1} + V_{\theta 2} \tag{11}$$

For $V_{\theta 1}$ the following empirical relation has been presented:

$$\frac{V_{\theta 1}}{r} = a\omega_0 \left(\frac{r - r_0}{R_0 - r_0} \right)^b \tag{12}$$

where a and b are empirical constants, and have been obtained as 0.2051 and -0.2947 respectively from the data of Kataoka[5] with the correlation coefficient -0.9848 for $0.1 \leqq (r-r_0)/(R_0-r_0) \leqq 0.9$ by using the least-squares method. When the inner shaft is at rest (i.e. $\omega_0 = 0$) the trajectory of particle (τ) must be straight in consistent with the jet direction AJ as shown in **Fig. 7**. In such a special case of $\omega_0 = 0$, we suppose that particle (τ) has reached point $J(r, \theta^*)$ at some instant t, and let V_r^* and $V_{\theta 2}^*$ be the radial and tangential velocity components respectively for particle (τ) at point J. Thus, the following relation must be satisfied:

$$V_{\theta 2}^* = V_r^* \tan(\theta_{in} - \theta^*) \tag{13}$$

This relation can be rewritten as (see **Appendix**)

$$V_{\theta 2}^* = V_r^* \frac{r_0 \sin\theta_{in}}{\sqrt{r^2 - (r_0 \sin\theta_{in})^2}} \tag{14}$$

Following Eq. (10), the radial velocity component at point $J(r, \theta^*)$, V_r^*, is equal to V_r at point $P(r, \theta)$. For simplicity, we assume that $V_{\theta 2}$ is equal to $V_{\theta 2}^*$. Substituting Eqs. (12) and (14) into Eq. (11), the following relation is obtained:

$$g(r) \equiv V_\theta = ar\omega_0 \left(\frac{r - r_0}{R - r_0} \right)^b + f(r) \frac{r_0 \sin\theta_{in}}{\sqrt{r^2 - (r_0 \sin\theta_{in})^2}} \tag{15}$$

Substitution of Eqs. (10) and (15) into (7) gives a correlation equation of the streak line at time T

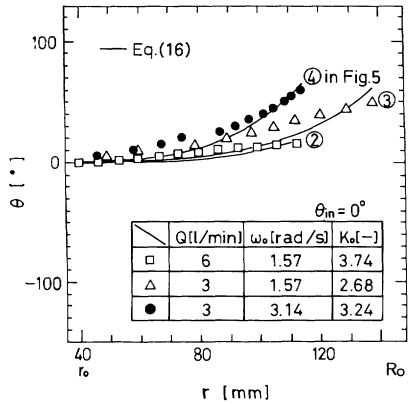

Fig. 8. Streak line for 0° nozzle angle with polar coordinates

$$\theta = \theta_{in} - \arcsin\left[\left(\frac{r_0}{r} \right) \sin(\theta_{in}) \right] + \omega_0 (T + F(r)) + \int_{r_0}^{r} \frac{a\omega_0 \{(r-r_0)/(R_0-r_0)\}^b}{V_{jr}(r_0/r)\exp\{-K_0(r-r_0)/(R_0-r_0)\}} dr \tag{16}$$

where

$$F(r) = \frac{1}{V_{jr}} \left(\frac{R_0 - r_0}{K_0} \right) \times \left[\frac{r}{r_0} \exp\left(K_0 \frac{r - r_0}{R_0 - r_0} \right) - 1 \right] - \frac{1}{V_{jr} r_0} \times \left(\frac{R_0 - r_0}{K_0} \right)^2 \left[\exp\left(K_0 \frac{r - r_0}{R_0 - r_0} \right) - 1 \right] \tag{17}$$

and

$$V_{jr} = V_j \cos\theta_{in} \tag{18}$$

The value of the empirical constant K_0 was determined by applying direct search by an optimal method to the experimental data. The value of K_0 depended upon nozzle angle, nozzle's rotating speed and direction of rotation, where

$$K_0 = \begin{cases} 2.84\text{–}3.15 & \text{at } \omega_0 > 0 \quad \text{for } \theta = 30^\circ \\ 5.27\text{–}7.68 & \text{at } \omega_0 < 0 \quad \text{for } \theta = 30^\circ \\ 2.68\text{–}3.74 & \text{for } \theta = 0^\circ \end{cases} \tag{19}$$

Figures 8 and **9** show the observed data of the streak lines with the polar coordinates (r, θ), where the solid lines in these figures show the theoretical lines calculated with Eq. (16). The circle and black circle keys show the operating conditions giving the minimum dimensionless mixing time, and the triangle and black triangle keys show the conditions giving the maximum dimensionless mixing time. The streak lines for the conditions ⑤ and ⑧, on which the dimensionless mixing times have almost the same values in Fig. 5, are almost symmetrical with respect to the axis of $\theta = 0$.

Figure 10 shows that streak lines determined by

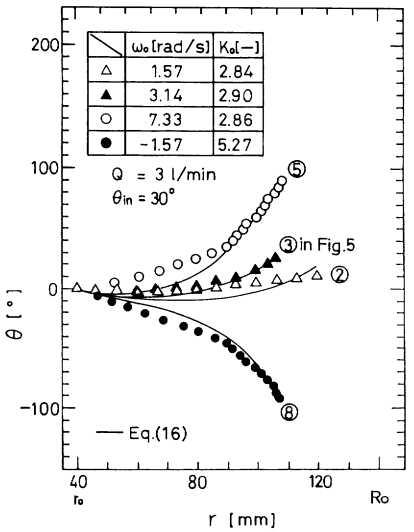

Fig. 9. Streak line for 30° nozzle angle with polar coordinates

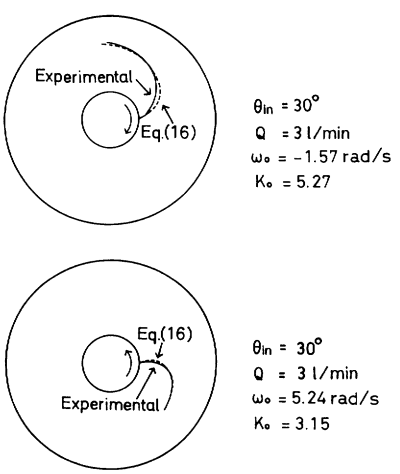

Fig. 10. Streak line of jet flow

using Eq. (16) with proper K_0 values compared favorably with visualized jet flows. From the correlation equation of streak lines with a correction factor, it is possible to estimate a flow pattern at an optional condition.

Conclusion

The observed jet angle from the visualization of jet flow was 21°–24° regardless of the jet flow rate.

With the start of nozzle rotation the front part of the bounded tangential jet in the direction of nozzle rotation interfered with the successive radial jet flow's impingement on the vessel wall. Consequently, the mixing efficiency was lowered and the dimensionless mixing time increased. The higher nozzle rotation made the radial jet bend in the tangential direction and the resultant jet is bound between shaft and vessel walls, where the minimum dimensionless mixing time occurred. Reverse rotation against the nozzle direction

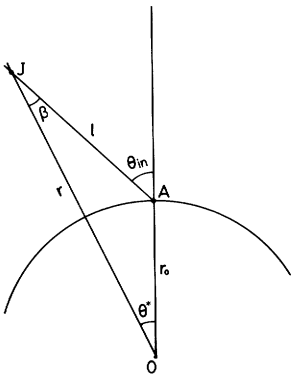

Fig. A.1. Relation of angles in the special case of $\omega_0=0$

gave the minimum dimensionless mixing time at a smaller dimensionless nozzle rotation speed, because the jet flow was assisted by a relative tangential flow produced by the nozzle rotation to an inner shaft rotation.

Streak lines calculated from a correlation equation with an empirical constant matched well with visualized jet flows.

Appendix Derivation of Eq. (14)

For the special case where the inner shaft is at rest, i.e. $\omega_0=0$, point A coincides with point S in Fig. 7, and consequently Fig. 7 reduces to **Fig. A.1**. The following relations are obtained for ΔAJO in Fig. A.1:

$$l\sin\beta = r_0\sin\theta^* \tag{A.1}$$

$$l\cos\beta + r_0\cos\theta^* = r \tag{A.2}$$

where

$$l\equiv AJ \quad \text{and} \quad \beta\equiv \angle AJO=\theta_{in}-\theta^* \tag{A.3}$$

Eliminating l from Eqs. (A.1) and (A.2), we get

$$r_0(\sin\theta^*\cos\beta+\sin\beta\cos\theta^*) = r_0\sin(\theta^*+\beta)=r\sin\beta \tag{A.4}$$

Considering the definition of β, i.e. Eq. (A.3), we obtain

$$\sin\beta\equiv\sin(\theta_{in}-\theta^*)=\frac{r_0\sin\theta_{in}}{r} \tag{A.5}$$

This relation can be changed to an equivalent form as

$$\tan\beta\equiv\tan(\theta_{in}-\theta^*)=\frac{r_0\sin\theta_{in}}{\sqrt{r^2-(r_0\sin\theta_{in})^2}} \tag{A.6}$$

Thus, Eq. (13) in the text can be rewritten as

$$V^*_{\theta 2}\equiv V^*_r\tan(\theta_{in}-\theta^*)=V^*_r\frac{r_0\sin\theta_{in}}{\sqrt{r^2-(r_0\sin\theta_{in})^2}} \tag{A.7}$$

This is Eq. (14) in the text.

Acknowledgement

The authors wish to thank Mr. Hideto Tange for his assistance.

Nomenclature

a	=	empirical constant in Eq. (12)	[—]
b	=	empirical constant in Eq. (12)	[—]

$f(r)$ = radial velocity component for particle (τ) [$m \cdot s^{-1}$]
$g(r)$ = tangential velocity component for particle (τ) [$m \cdot s^{-1}$]
H = liquid height [m]
K = correction factor in Eq. (8) [—]
K_0 = empirical constant in Eq. (9) [—]
Q = jet flow rate [l/min]
R_0 = radius of mixing vessel [m]
r = radial distance from center of inner shaft [m]
r_0 = radius of inner shaft [m]
t = time [s]
t_0 = starting time for taking first photograph [s]
t_M = mixing time [s]
t_n = time elapsed from t_0, ($t_n = n \times 0.29$ s) [s]
t_R = residence time [s]
V_j = jet velocity at jet nozzle exit [$m \cdot s^{-1}$]
V_r = radial velocity component at $P(r, \theta)$ in Fig. 7 [$m \cdot s^{-1}$]
V_{jr} = radial velocity component at jet nozzle exit [$m \cdot s^{-1}$]
V_r^* = radial velocity component at $J(r, \theta^*)$ in Fig. 7 [$m \cdot s^{-1}$]
V_θ = tangential velocity component at $P(r, \theta)$ in Fig. 7 [$m \cdot s^{-1}$]
$V_{\theta 1}$ = tangential velocity induced by rotation of inner shaft [$m \cdot s^{-1}$]
$V_{\theta 2}$ = tangential velocity induced by jet flow at $P(r, \theta)$ in Fig. 7 [$m \cdot s^{-1}$]
$V_{\theta 2}^*$ = tangential velocity induced by jet flow at $J(r, \theta^*)$ in Fig. 7 [$m \cdot s^{-1}$]

θ = angle in polar coordinates system [rad]
θ_{in} = nozzle angle (see Fig. 7) [rad]
τ = time elapsed from $t = 0$ (see Fig. 6) [s]
ω_0 = angular velocity of inner shaft [$rad \cdot s^{-1}$]
Ω^* = dimensionless nozzle rotation speed ($\equiv \omega_0 r_0 / V_j$) [—]

Literature Cited

1) Abramovich, G. N.: "The Theory of Turbulent Jets", Mass. Inst. Technol. Press, Cambridge (1963).
2) Chesters, J. H., I. M. D. Halliday and R. S. Howes: "Some Aspects of Fluid Flow", pp. 176–193, Arnold Press, London (1951).
3) Ferguson, C. K. and R. G. Folsom: *Trans. Amer. Soc. Mech. Engrs.*, **71**, 73 (1949).
4) Folsom, R. G.: *Proc. Nat. Conf. Ind. Hydraul.* (1948).
5) Kataoka, K.: Ph. D. Thesis, Tokyo Univ., Japan (1970).
6) Koh, S. T., S. Hiraoka, Y. Tada, T. Takahashi, T. Aragaki and I. Yamada: *J. Chem. Eng. Japan*, **23**, 462 (1990).
7) Koh, S. T., S. Hiraoka, Y. Tada, T. Aragaki, I. Yamada, T. Takahashi and K. Suzuki: *J. Chem. Eng. Japan*, **23**, 627 (1990).
8) Konig, G. and A. Frohn: *Flow Visualization, Proc. Int. Symp.*, 3rd. 488 (1983).
9) Lane, A. G. C. and P. Rice: *Trans. IChemE.* **60**, 245 (1982).
10) Mathur, M. L. and N. R. L. Maccallum: *Journal of the Institute of Fuel*, June, 238 (1967).
11) Nienow, A. W. and R. Kuboi: *Inst. Chem. Eng. Symp. Ser.* No. 89 (Fluid Mixing), p. 97 (1984).
12) Pearce, A. F.: CSIR Report, Pretoria, South Africa, MEG 475 (1966).
13) Revill, B. K.: "Mixing in the Process Industries", Butterworth & Co., Ltd., London (1985).
14) Rubach, H. L.: "Handbook of Flow Visualization", p. 169, Asakura Press, Tokyo (1977).
15) Sato, K.: *Kagaku Kogaku*, **32**, 588 (1968).